International Journal of Solids and Structures 51 (2014) 3480–3489

Contents lists available at ScienceDirect

International Journal of Solids and Structures

journal homepage: www.elsevier.com/locate/ijsolstr

Regularization of microplane damage models using an implicit gradient enhancement

Imadeddin Zreid, Michael Kaliske *

Institute for Structural Analysis, Technische Universität Dresden, 01062 Dresden, Germany

ARTICLE INFO

Article history:
Received 4 April 2014
Received in revised form 28 May 2014
Available online 1 July 2014

Keywords:
Microplane model
Damage
Implicit gradient enhancement
Concrete

ABSTRACT

The microplane model allows for the description of damage induced anisotropy in a natural manner by introducing constitutive laws for quantities on individual microplanes at each material point. However, if damage or other strain softening constitutive laws are used within the microplane approach, the well-known problem of localization arises leading to spurious results and mesh dependency. This problem demands some regularization method to stabilize the solution. The paper focuses on the efficient implementation of implicit gradient enhancement for microplane damage models. Previous works enhanced the strain tensor, thus resulting in large number of extra degrees of freedom, which limits the use of this method for large scale 3D simulations. A new method which enhances the equivalent strain driving the damage on each microplane is introduced in this work. The new method limits the number of additional degrees of freedom to one, while preserving the regularizing effect. The two methods are implemented within a 3D finite element code to compare their performance. The microplane model used is based on a thermodynamically consistent formulation and on a volumetric–deviatoric split of strains on each microplane. Furthermore, an exponential damage law is used and an equivalent strain expression which distinguishes between compression and tension is applied to simulate the behavior of concrete. The capabilities of the proposed formulation are demonstrated by comparison to published experiments on plain concrete.

1. Introduction

The microplane model is a powerful tool for modeling concrete and other quasi-brittle materials (Bažant et al., 2000; Caner and Bažant, 2013a). The behavior of those materials is characterized by the transition from isotropic to anisotropic response once the material enters the inelastic regime. Concrete, for example, which consists of different constituents, exhibits upon loading initiation of microcracks often at the interfaces between aggregates and the mortar matrix. The growth of these microcracks leads to anisotropic behavior and eventually to macroscopic cracks and failure. The microplane approach provides a simple and straightforward way to model this phenomenon by defining the constitutive material relations between stress and strain vectors on randomly oriented planes. Since the pioneering work by Bažant and Prat (1988), it has been researched extensively, and a variety of constitutive material laws has been implemented within the microplane approach including damage and plasticity. However, the strain localization problem which is well known for strain softening constitutive models persists also with microplane models. This problem is caused by ill-posedness of the governing differential equations in case of strain softening material laws, which leads to pathological mesh dependency and numerical instability of the finite element solution.

Many remedies have been proposed to counter this problem and some of them have been already used to regularize microplane damage models. One powerful and physically motivated method is the nonlocal integral type approach. Although usually motivated by its ability to eliminate mesh dependency and slow convergence rate, micromechanical arguments have been also presented. For example, the dependency of damage at one microcrack on the release of stored energy from its neighborhood, and the effect of material inhomogeneity, which causes the dependency of the stress state at a given material point on its surrounding region (Bažant, 1991). One difficulty with the integral type formulation is that it leads to a set of integro-differential equations, which require sharing information between points, thus abandoning the advantage of classical finite element method and complicating

* Corresponding author. Tel.: +49 351 463 34386.
E-mail address: michael.kaliske@tu-dresden.de (M. Kaliske).

http://dx.doi.org/10.1016/j.ijsolstr.2014.06.020
0020-7683/

the implementation within the finite element software. This issue motivated the so-called gradient enhanced models, which preserve the mathematical locality of the finite element method, while taking the field around the point into account by enhancing the equations with higher gradients of strain or other internal variables. There are two types of gradient models, explicit and implicit. Explicit gradient enhancement is only weakly nonlocal, thus fails to regularize the solution under some circumstances. Implicit gradient enhancement, on the other hand, have the advantage of being strongly nonlocal and largely equivalent to the integral type (Peerlings et al., 2001), while keeping the differential nature of the equations, thus results in a straightforward implementation in finite element codes. Its idea is to introduce a second differential equation to calculate the nonlocal field, which is usually the counterpart of the local strain or other local internal variables. The expense to be paid in this case is adding extra degrees of freedom. For isotropic damage models, it is sufficient to apply the enhancement for a scalar valued quantity, such as the equivalent strain (Saroukhani et al., 2013), thus the extra degrees of freedom is limited to 1. This fact makes implicit gradient enhancement for isotropic damage models very successful. On the other hand, for anisotropic models, the nonlocal field needs to be a tensorial quantity, or in case of microplane models a scalar quantity at every microplane. This problem means that the number of extra degrees of freedom is very large and renders the method unpractical for large scale 3D simulations.

Though the microplane model has been researched extensively, little attention has been paid to the regularizing techniques which are essential for the practical application of the model (Caner and Bažant, 2013a). A nonlocal integral type method has been implemented for the microplane model, for instance, in Bažant and Di Luzio (2004), Bažant and Ozbolt (1990) and Luzio (2007). Implicit gradient enhanced microplane models have been introduced in Kuhl et al. (2000) and Leukart (2005), where the strain tensor has been used as the nonlocal variable. The aim of this work is to explore the feasibility of formulating an efficient and reliable way to regularize the microplane damage models using an implicit gradient enhancement. The paper is organized as follows. Firstly, the gradient model used in Kuhl et al. (2000) and Leukart (2005) is reviewed and explained. Afterwards, a new simplified method for the implicit gradient enhancement is derived. Finally, the behavior of the two methods is demonstrated and compared by simulations of experiments on plain concrete.

2. Strain gradient model

2.1. Finite element formulation

The gradient enhanced microplane damage model in Kuhl et al. (2000) and Leukart (2005) is based on enhancing the strain tensor. This means that a tensorial nonlocal field is considered. The system is then governed by 2 coupled differential equations and solved using a simultaneous, fully coupled scheme. The first equation is balance of linear momentum for quasi-static case

$$\nabla \cdot \boldsymbol{\sigma} + \boldsymbol{f} = 0 \tag{1}$$

and the second is the modified Helmholtz equation to describe the nonlocal strain tensor

$$\bar{\boldsymbol{\epsilon}} - c\nabla^2 \bar{\boldsymbol{\epsilon}} = \boldsymbol{\epsilon}, \tag{2}$$

with the homogenous Neumann boundary condition

$$\nabla \bar{\boldsymbol{\epsilon}} \cdot \boldsymbol{n}_b = \boldsymbol{0}, \tag{3}$$

where, $\boldsymbol{\sigma}$ is the Cauchy stress tensor, $\nabla\cdot$ is the divergence operator and $\boldsymbol{f}$ is the body force vector. Moreover, $\boldsymbol{\epsilon}$ is the local strain tensor, $\bar{\boldsymbol{\epsilon}}$ is its nonlocal counterpart, c is the gradient activity parameter, $\boldsymbol{n}_b$ is the normal to the outer boundary, ∇ is the gradient operator and ∇^2 is the Laplace operator.

The homogenous Neumann boundary condition adopted here is commonly used and it is enough to ensure the regularizing effect. With this boundary condition the local and nonlocal strains are equal for homogenous deformations and the gradient method is, therefore, consistent with integral type formulation. Peerlings et al. (2001) showed that this type of boundary condition provides larger nonlocal weight factors for the material close to the external boundaries. This is motivated from the physical point of view, because the model in this case will be more sensitive to surface effects. This boundary condition is applied to the entire external boundary regardless whether there are applied displacements or loads to some regions or not, since a physical connection between the two fields boundaries is not clear.

To get the weak form of Eqs. (1) and (2), they are multiplied by the weight functions $\delta\mathbf{u}$ and $\delta\bar{\boldsymbol{\epsilon}}$, respectively,

$$\int_{\mathcal{B}} \delta\mathbf{u} \cdot \nabla \cdot \boldsymbol{\sigma} dv + \int_{\mathcal{B}} \delta\mathbf{u} \cdot \boldsymbol{f} dv = 0, \tag{4}$$

$$\int_{\mathcal{B}} \delta\bar{\boldsymbol{\epsilon}} \cdot \bar{\boldsymbol{\epsilon}} dv - \int_{\mathcal{B}} \delta\bar{\boldsymbol{\epsilon}} \cdot c\nabla^2 \bar{\boldsymbol{\epsilon}} dv = \int_{\mathcal{B}} \delta\bar{\boldsymbol{\epsilon}} \cdot \boldsymbol{\epsilon} dv. \tag{5}$$

Substituting the relation $\nabla \cdot (\boldsymbol{\sigma} \cdot \delta\mathbf{u}) = \delta\mathbf{u} \cdot \nabla \cdot \boldsymbol{\sigma} + \boldsymbol{\sigma} : \nabla\delta\mathbf{u}$, Gauss divergence theorem $\int_{\partial\mathcal{B}} \boldsymbol{\sigma}\boldsymbol{n}_b \cdot \delta\mathbf{u} da = \int_{\mathcal{B}} \nabla \cdot (\boldsymbol{\sigma} \cdot \delta\mathbf{u}) dv$ and Cauchy theorem $\boldsymbol{\sigma} \cdot \boldsymbol{n}_b = \mathbf{t}_e$ in Eq. (4) yield

$$\int_{\partial\mathcal{B}} \mathbf{t}_e \cdot \delta\mathbf{u} da - \int_{\mathcal{B}} \boldsymbol{\sigma} : \nabla\delta\mathbf{u} dv = \int_{\mathcal{B}} \delta\mathbf{u} \cdot \boldsymbol{f} dv \tag{6}$$

and similarly for Eq. (5), substituting the relation $\nabla \cdot (\delta\bar{\boldsymbol{\epsilon}} \cdot \nabla\bar{\boldsymbol{\epsilon}}) = \delta\bar{\boldsymbol{\epsilon}} \cdot \nabla^2\bar{\boldsymbol{\epsilon}} + \nabla\delta\bar{\boldsymbol{\epsilon}} \cdot \nabla\bar{\boldsymbol{\epsilon}}$, Gauss divergence theorem $\int_{\partial\mathcal{B}} \nabla\bar{\boldsymbol{\epsilon}} \cdot \boldsymbol{n}_b \cdot \delta\bar{\boldsymbol{\epsilon}} da = \int_{\mathcal{B}} \nabla \cdot (\delta\bar{\boldsymbol{\epsilon}} \cdot \nabla\bar{\boldsymbol{\epsilon}}) dv$ and the boundary condition $\nabla\bar{\boldsymbol{\epsilon}} \cdot \boldsymbol{n}_b = 0$ yield

$$\int_{\mathcal{B}} \delta\bar{\boldsymbol{\epsilon}} \cdot \bar{\boldsymbol{\epsilon}} dv + \int_{\mathcal{B}} \nabla\delta\bar{\boldsymbol{\epsilon}} \cdot c\nabla\bar{\boldsymbol{\epsilon}} dv = \int_{\mathcal{B}} \delta\bar{\boldsymbol{\epsilon}} \cdot \boldsymbol{\epsilon} dv. \tag{7}$$

Space discretization for the finite element method is obtained by dividing the domain $\mathcal{B}$ into sub-domains $\mathcal{B}^e \subset \mathcal{B}$. Interpolation within the elements is achieved with eight nodes using linear shape functions $\boldsymbol{N}(\xi, \eta, \zeta)$ within the isoparametric concept of finite element method, where ξ, η and ζ are local coordinates that can have values from -1 to 1. Then, the displacement field, and the variational field $\delta\mathbf{u}$ may be interpolated over the sub-domains as follows

$$\mathbf{u} = \boldsymbol{N}(\xi, \eta, \zeta)\boldsymbol{d}^e, \quad \delta\mathbf{u}(\xi, \eta, \zeta) = \boldsymbol{N}(\xi, \eta, \zeta)\delta\boldsymbol{d}^e \tag{8}$$

and the gradient of the displacement field is given as

$$\nabla\mathbf{u} = \partial_{\mathbf{x}}\boldsymbol{N}\boldsymbol{d}^e = \boldsymbol{B}\boldsymbol{d}^e, \quad \nabla\delta\mathbf{u} = \partial_{\mathbf{x}}\boldsymbol{N}\delta\boldsymbol{d}^e = \boldsymbol{B}\delta\boldsymbol{d}^e. \tag{9}$$

Similarly, the nonlocal strain field and its variational field are also interpolated with linear shape functions $\overline{\boldsymbol{N}}$ as follows

$$\bar{\boldsymbol{\epsilon}} = \overline{\boldsymbol{N}}\boldsymbol{E}^e, \quad \delta\bar{\boldsymbol{\epsilon}} = \overline{\boldsymbol{N}}\delta\boldsymbol{E}^e \tag{10}$$

and the gradient of the nonlocal field is given as

$$\nabla\bar{\boldsymbol{\epsilon}} = \partial_{\mathbf{x}}\overline{\boldsymbol{N}}\boldsymbol{E}^e = \overline{\boldsymbol{B}}\boldsymbol{E}^e, \quad \nabla\delta\bar{\boldsymbol{\epsilon}} = \partial_{\mathbf{x}}\overline{\boldsymbol{N}}\delta\boldsymbol{E}^e = \overline{\boldsymbol{B}}\delta\boldsymbol{E}^e, \tag{11}$$

where $\boldsymbol{d}^e$ are the nodal displacements and $\boldsymbol{E}^e$ are the nodal nonlocal strains. The equations have to be satisfied for all admissible $\delta\boldsymbol{d}^e$ and $\delta\boldsymbol{E}^e$, so finally Eqs. (6) and (7) become

$$\int_{\mathcal{B}} \boldsymbol{B}^T\boldsymbol{\sigma} dv = \int_{\mathcal{B}} \boldsymbol{N}^T\boldsymbol{f} dv + \int_{\partial\mathcal{B}_e} \boldsymbol{N}^T\mathbf{t}_e da, \tag{12}$$

$$\int_{\mathcal{B}} \overline{\boldsymbol{N}}^T\bar{\boldsymbol{\epsilon}} dv + \int_{\mathcal{B}} \overline{\boldsymbol{B}}^T c\nabla\bar{\boldsymbol{\epsilon}} dv = \int_{\mathcal{B}} \overline{\boldsymbol{N}}^T\boldsymbol{\epsilon} dv. \tag{13}$$

2.2. Linearization

Eqs. (12) and (13) should be linearized, in order to be solved by an incremental iterative Newton–Raphson solution. The residual expression of the previous system of equations may be written as

$$\mathbf{R}^e = \begin{bmatrix} \mathbf{R}^e_u \\ \mathbf{R}^e_{\bar{\epsilon}} \end{bmatrix} = \begin{bmatrix} \boldsymbol{f}^{ext}_u \\ \boldsymbol{f}^{ext}_{\bar{\epsilon}} \end{bmatrix} - \begin{bmatrix} \boldsymbol{f}^{int}_u \\ \boldsymbol{f}^{int}_{\bar{\epsilon}} \end{bmatrix}. \tag{14}$$

These equations are nonlinear in the unknown solution vector $\mathbf{X}^e = \begin{bmatrix} \boldsymbol{d}^e & \boldsymbol{E}^e \end{bmatrix}^T$ of all degrees of freedom. Linearization yields

$$\mathrm{Lin}\,\mathbf{R}^e = \mathbf{R}^e\big|_{\mathbf{X}^e,i} + \left(\frac{\partial \mathbf{R}^e}{\partial \mathbf{X}^e}\right)\Big|_{\mathbf{X}^e,i} \cdot \triangle \mathbf{X}^e_{,i+1}, \tag{15}$$

where $i+1$ is the current time step. The fully coupled simultaneous solution takes the form

$$\begin{bmatrix} \mathbf{K}^e_{uu,i} & \mathbf{K}^e_{u\bar{\epsilon},i} \\ \mathbf{K}^e_{\bar{\epsilon}u,i} & \mathbf{K}^e_{\bar{\epsilon}\bar{\epsilon},i} \end{bmatrix} \begin{bmatrix} \Delta \boldsymbol{d}^e_{,i+1} \\ \Delta \boldsymbol{E}^e_{,i+1} \end{bmatrix} = - \begin{bmatrix} \mathbf{R}^e_{u,i} \\ \mathbf{R}^e_{\bar{\epsilon},i} \end{bmatrix}, \tag{16}$$

where the residual vectors are

$$\mathbf{R}^e_{u,i} = \int_{\mathcal{B}} \boldsymbol{B}^T \boldsymbol{\sigma} dv - \int_{\mathcal{B}} \boldsymbol{N}^T \boldsymbol{f} dv - \int_{\partial \mathcal{B}_e} \boldsymbol{N}^T \mathbf{t}_e da, \tag{17}$$

$$\mathbf{R}^e_{\bar{\epsilon},i} = \int_{\mathcal{B}} \overline{\boldsymbol{B}}^T c \overline{\boldsymbol{B}} \boldsymbol{E}^e dv + \int_{\mathcal{B}} \overline{\boldsymbol{N}}^T \left[\overline{\boldsymbol{N}} \boldsymbol{E}^e - \boldsymbol{B} \boldsymbol{d}^e\right] dv \tag{18}$$

and the submatrices of the consistent stiffness matrix

$$\mathbf{K}^e_{uu,i} = \frac{\partial}{\partial \boldsymbol{d}^e} \mathbf{R}^e_{u,i} = \int_{\mathcal{B}} \boldsymbol{B}^T \frac{\partial \boldsymbol{\sigma}}{\partial \boldsymbol{\epsilon}} \boldsymbol{B} dv, \tag{19}$$

$$\mathbf{K}^e_{u\bar{\epsilon},i} = \frac{\partial}{\partial \boldsymbol{E}^e} \mathbf{R}^e_{u,i} = \int_{\mathcal{B}} \boldsymbol{B}^T \frac{\partial \boldsymbol{\sigma}}{\partial \bar{\boldsymbol{\epsilon}}} \overline{\boldsymbol{N}} dv, \tag{20}$$

$$\mathbf{K}^e_{\bar{\epsilon}u,i} = \frac{\partial}{\partial \boldsymbol{d}^e} \mathbf{R}^e_{\bar{\epsilon},i} = - \int_{\mathcal{B}} \overline{\boldsymbol{N}}^T \boldsymbol{B} dv, \tag{21}$$

$$\mathbf{K}^e_{\bar{\epsilon}\bar{\epsilon},i} = \frac{\partial}{\partial \boldsymbol{E}^e} \mathbf{R}^e_{\bar{\epsilon},i} = \int_{\mathcal{B}} \overline{\boldsymbol{B}}^T c \overline{\boldsymbol{B}} dv + \int_{\mathcal{B}} \overline{\boldsymbol{N}}^T \overline{\boldsymbol{N}} dv. \tag{22}$$

2.3. Microplane damage model

Many microplane models exist in the literature with different types of strain and stress splits and a variety of constitutive laws. Here, the model proposed in Leukart (2005) is adopted, which is based on a volumetric–deviatoric (V–D) split of strains and formulated in a thermodynamically consistent way. The model applies the kinematic constraint, i.e. the microplane strains are assumed to be equal to the projection of the macroscopic strain tensor to the microplanes, not stresses as assumed in case of static constraint. Furthermore, the damage is considered with one damage parameter applied for both the volumetric and the deviatoric parts of the stresses. Although, the volumetric and deviatoric damages are different and using one damage law is not the best way to model concrete, this version is still a simple and robust version of the microplane model. It also gives some kind of deviatoric-volumetric coupling, which is usually ignored by the 2 damage parameters models. The macroscopic free energy is computed as the integral of microplane free energies over the solid angle Ω,

$$\Psi^{mac} = \frac{3}{4\pi} \int_{\Omega} \Psi^{mic} d\Omega \tag{23}$$

and the free energy at the microplane level is defined as

$$\Psi^{mic} = \left[1 - d^{mic}\right] \left[\frac{1}{2} K^{mic} \epsilon_V^2 + G^{mic} \boldsymbol{\epsilon}_D \cdot \boldsymbol{\epsilon}_D\right], \tag{24}$$

where d^{mic} is the damage variable at each microplane and ϵ_V and $\boldsymbol{\epsilon}_D$ are the volumetric and deviatoric microplane strains, respectively. They are computed by projecting the macroscopic strain tensor to microplanes as follows

$$\epsilon_V = \boldsymbol{V} \boldsymbol{\epsilon}, \quad \boldsymbol{\epsilon}_D = \boldsymbol{Dev} \cdot \boldsymbol{\epsilon}, \tag{25}$$

where the projection tensors $\boldsymbol{V}$ and $\boldsymbol{Dev}$ are defined knowing the normal vector $\boldsymbol{n}$ to each microplane as

$$\boldsymbol{V} = \frac{1}{3}\mathbf{1}, \quad \boldsymbol{Dev} = \boldsymbol{n} \cdot \mathbf{I}^{dev} = \boldsymbol{n} \cdot \mathbf{I}^{sym} - \frac{1}{3} \boldsymbol{n} \cdot \mathbf{1} \otimes \mathbf{1}, \tag{26}$$

$$\boldsymbol{Dev}^T = \mathbf{I}^{dev} \cdot \boldsymbol{n}, \tag{27}$$

where $\mathbf{1}$ is the second order identity tensor, $\mathbf{I}$ is the fourth order identity tensor and $\mathbf{I}^{sym} = \frac{1}{2}\left[\mathbf{I} + \mathbf{I}^T\right]$ is its symmetric part. Furthermore, the elastic material parameters K^{mic} and G^{mic} are related to the elastic macroscopic parameters as follows

$$K^{mic} = 3K, \quad G^{mic} = G. \tag{28}$$

The evolution law of the damage variable d^{mic} is an exponential law (Geers et al., 1998),

$$d^{mic} = 1 - \frac{\gamma_0}{\gamma^{mic}} \left[1 - \alpha + \alpha \exp\left[\beta\left[\gamma_0 - \gamma^{mic}\right]\right]\right], \tag{29}$$

where α, β and γ_0 are positive material parameters. α represents the maximum degradation of the material, β controls the shape of softening, and γ_0 is the damage threshold. Fig. 1 shows the law graphically. The damage evolution is driven with the history variable γ^{mic}, which represents the largest value of equivalent strain that has ever occurred in the whole loading history up to the current time step t. This may be expressed as

$$\gamma^{mic}(t) = \max_{\tau \leqslant t} (\gamma_0, \eta^{mic}(\tau)). \tag{30}$$

The equivalent strain at each microplane η^{mic} is computed as in de and Brekelmans (1995). This is a modified form of von Mises equivalent strain to distinguish compression from tension, which is an essential property of concrete,

$$\eta^{mic} = 3k_1 \bar{\epsilon}_V + \sqrt{(3k_1 \bar{\epsilon}_V)^2 + \frac{3}{2} k_2 \bar{\boldsymbol{\epsilon}}_D \cdot \bar{\boldsymbol{\epsilon}}_D}. \tag{31}$$

Note that unlike the local model, the equivalent strain now is a function of the nonlocal stress tensor $\eta^{mic} = f(\bar{\boldsymbol{\epsilon}})$. The components $\bar{\epsilon}_V$ and $\bar{\boldsymbol{\epsilon}}_D$ are computed by projecting the nonlocal strain tensor $\bar{\boldsymbol{\epsilon}}$ to microplanes,

$$\bar{\epsilon}_V = \boldsymbol{V} \bar{\boldsymbol{\epsilon}}, \quad \bar{\boldsymbol{\epsilon}}_D = \boldsymbol{Dev} \cdot \bar{\boldsymbol{\epsilon}} \tag{32}$$

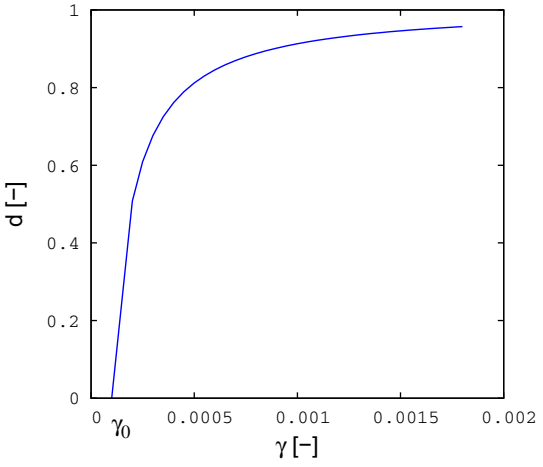

Fig. 1. Exponential damage evolution law.

and the constants k_1 and k_2 are computed from material parameters, namely Poisson's ratio ν and the ratio between the compressive and tensile strength as follows

$$k_1 = \frac{k_r - 1}{2k_r(1-2\nu)}, \tag{33}$$

$$k_2 = \frac{3}{k_r(1+\nu)^2}. \tag{34}$$

The stress tensor can be found by taking the free energy derivative with respect to the strain tensor,

$$\boldsymbol{\sigma} = \frac{\partial \Psi^{mac}}{\partial \boldsymbol{\epsilon}} = \frac{3}{4\pi}\int_\Omega \left[1-d^{mic}\right]\left[K^{mic}\boldsymbol{V}\epsilon_V + 2G^{mic}\boldsymbol{Dev}^T\cdot\boldsymbol{\epsilon}_D\right]d\Omega \tag{35}$$

and the tangent terms

$$\mathbb{C} = \frac{\partial \boldsymbol{\sigma}}{\partial \boldsymbol{\epsilon}} = \frac{3}{4\pi}\int_\Omega \left[1-d^{mic}\right]\left[K^{mic}\boldsymbol{V}\otimes\boldsymbol{V} + 2G^{mic}\boldsymbol{Dev}^T\cdot\boldsymbol{Dev}\right]d\Omega, \tag{36}$$

$$\overline{\mathbb{C}} = \frac{\partial \boldsymbol{\sigma}}{\partial \bar{\boldsymbol{\epsilon}}} = -\frac{3}{4\pi}\int_\Omega \frac{\partial d^{mic}}{\partial \gamma^{mic}}\frac{\partial \gamma^{mic}}{\partial \eta^{mic}}\left[K^{mic}\boldsymbol{V}\epsilon_V + 2G^{mic}\boldsymbol{Dev}^T\boldsymbol{\epsilon}_D\right]\otimes\frac{\partial \eta^{mic}}{\partial \bar{\boldsymbol{\epsilon}}}d\Omega, \tag{37}$$

where the required derivatives are

$$\frac{\partial d^{mic}}{\partial \gamma^{mic}} = \frac{\gamma_0}{(\gamma^{mic})^2}\left(1-\alpha+\alpha\exp\left(\beta(\gamma_0-\gamma^{mic})\right)\right) \tag{38}$$

$$+\frac{\gamma_0}{\gamma^{mic}}\alpha\beta\exp\left(\beta(\gamma_0-\gamma^{mic})\right), \tag{39}$$

$$\frac{\partial \gamma^{mic}}{\partial \eta^{mic}} = \begin{cases} 1 & \text{if} \quad \gamma^{mic}(t) = \eta^{mic}(t), \\ 0 & \text{otherwise}, \end{cases} \tag{40}$$

$$\frac{\partial \eta^{mic}}{\partial \bar{\boldsymbol{\epsilon}}} = 3k_1\boldsymbol{V} + \frac{1}{2\sqrt{(3k_1\bar{\epsilon}_V)^2 + \frac{3}{2}k_2\bar{\boldsymbol{\epsilon}}_D\cdot\bar{\boldsymbol{\epsilon}}_D}}\left(18k_1^2\bar{\epsilon}_V\boldsymbol{V} + 3k_2\boldsymbol{Dev}^T\cdot\bar{\boldsymbol{\epsilon}}_D\right). \tag{41}$$

Note that in this method the elastic part of the model is not affected by the gradient enhancement. The nonlocal field is only present in the damage evolution law.

Regarding the integration over the surface of the sphere to calculate the homogenized stress tensor and stiffness matrix for the microplane model, numerical integration is used in this work according to Bažant and Oh (1986). Here, the integration is computed with 42 microplanes, but due to symmetries, it is enough to use 21 microplanes as follows

$$\frac{3}{4\pi}\int_\Omega (\bullet)d\Omega = \sum_{mic=1}^{21}(\bullet)w^{mic},$$

where w^{mic} is the weight for each integration point. Table 2 in Appendix A gives the coordinates and weight coefficients of the integration points.

3. A model with gradient of equivalent strain

This method is commonly used for isotropic damage models (Geers et al., 2000), but was avoided for microplane models, because this kind of models involves large number of microplanes with independent internal variables, which means a large number of degrees of freedom. The newly proposed method uses the equivalent strain of one microplane as the nonlocal field, thus the modified Helmholtz equation becomes

$$\bar{\eta}_m - c\nabla^2\bar{\eta}_m = \eta_m, \tag{42}$$

also with the homogeneous Neumann boundary condition

$$\nabla\bar{\eta}_m\cdot\boldsymbol{n}_b = 0, \tag{43}$$

where η_m is the equivalent strain of one microplane and $\bar{\eta}_m$ is its nonlocal counterpart. Choosing the suitable microplane is discussed later in this section. The computational gain of the new method is very substantial, since only one extra DOF is required. This means, for 3D simulations, solving a system of 4 DOF per node, compared to solving a 9 DOF system per node in case of the method explained in the previous section. Discretization of the previous differential equation yields

$$\int_\mathcal{B}\overline{\boldsymbol{N}}^T\bar{\eta}_m dv + \int_\mathcal{B}\overline{\boldsymbol{B}}^T c\nabla\bar{\eta}_m dv = \int_\mathcal{B}\overline{\boldsymbol{N}}^T\eta_m dv. \tag{44}$$

Following similar steps as explained in Section 2. The residual expression of the problem may be written as

$$\mathbf{R}^e = \begin{bmatrix}\mathbf{R}^e_u \\ \mathbf{R}^e_{\bar{\eta}}\end{bmatrix} = \begin{bmatrix}\boldsymbol{f}^{ext}_u \\ \boldsymbol{f}^{ext}_{\bar{\eta}}\end{bmatrix} - \begin{bmatrix}\boldsymbol{f}^{int}_u \\ \boldsymbol{f}^{int}_{\bar{\eta}}\end{bmatrix} \tag{45}$$

and the fully coupled simultaneous solution

$$\begin{bmatrix}\mathbf{K}^e_{uu,i} & \mathbf{K}^e_{u\bar{\eta},i} \\ \mathbf{K}^e_{\bar{\eta}u,i} & \mathbf{K}^e_{\bar{\eta}\bar{\eta},i}\end{bmatrix}\begin{bmatrix}\Delta\boldsymbol{d}^e_{,i+1} \\ \Delta\boldsymbol{E}^e_{,i+1}\end{bmatrix} = -\begin{bmatrix}\mathbf{R}^e_{u,i} \\ \mathbf{R}^e_{\bar{\eta},i}\end{bmatrix}, \tag{46}$$

where the residual vectors are

$$\mathbf{R}^e_{u,i} = \int_\mathcal{B}\boldsymbol{B}^T\boldsymbol{\sigma}dv - \int_\mathcal{B}\boldsymbol{N}^T\boldsymbol{f}dv - \int_{\partial\mathcal{B}_e}\boldsymbol{N}^T\mathbf{t}_e da, \tag{47}$$

$$\mathbf{R}^e_{\bar{\eta},i} = \int_\mathcal{B}\overline{\boldsymbol{B}}^T c\overline{\boldsymbol{B}}\boldsymbol{E}^e dv + \int_\mathcal{B}\overline{\boldsymbol{N}}^T\left[\overline{\boldsymbol{N}}\boldsymbol{E}^e - \eta_m\right]dv \tag{48}$$

and the stiffness submatrices are

$$\mathbf{K}^e_{uu,i} = \frac{\partial}{\partial \boldsymbol{d}^e}\mathbf{R}^e_{u,i} = \int_\mathcal{B}\boldsymbol{B}^T\frac{\partial\boldsymbol{\sigma}}{\partial\boldsymbol{\epsilon}}\boldsymbol{B}dv, \tag{49}$$

$$\mathbf{K}^e_{u\bar{\eta},i} = \frac{\partial}{\partial \boldsymbol{E}^e}\mathbf{R}^e_{u,i} = \int_\mathcal{B}\boldsymbol{B}^T\frac{\partial\boldsymbol{\sigma}}{\partial\bar{\eta}_m}\overline{\boldsymbol{N}}dv, \tag{50}$$

$$\mathbf{K}^e_{\bar{\eta}u,i} = \frac{\partial}{\partial \boldsymbol{d}^e}\mathbf{R}^e_{\bar{\eta},i} = -\int_\mathcal{B}\overline{\boldsymbol{N}}^T\frac{\partial\eta_m}{\partial\boldsymbol{\epsilon}}\boldsymbol{B}dv, \tag{51}$$

$$\mathbf{K}^e_{\bar{\eta}\bar{\eta},i} = \frac{\partial}{\partial \boldsymbol{E}^e}\mathbf{R}^e_{\bar{\eta},i} = \int_\mathcal{B}\overline{\boldsymbol{B}}^T c\overline{\boldsymbol{B}}dv + \int_\mathcal{B}\overline{\boldsymbol{N}}^T\overline{\boldsymbol{N}}dv. \tag{52}$$

Note that the element stiffness matrix is nonsymmetric since $\mathbf{K}^e_{u\bar{\eta}} \neq \mathbf{K}^e_{\bar{\eta}u}$, which is the case for coupled systems in general, therefore a nonsymmetric solver is required. However, this is not only the case for the new method, but also for the previous strain gradient method. Moreover, it cannot be considered a drawback only for the implicit gradient enhancement, since even local damage models have often nonsymmetric stiffness matrices. Only in special cases, a symmetric tangent matrix is achieved (Jirásek and Patzák, 2002).

The microplane chosen for the gradient enhancement is the one with the largest equivalent strain of the 21 microplanes used to approximate the integration,

$$\eta_m = \max_{mic=1}^{21}(\eta^{mic}) \tag{53}$$

and its nonlocal counterpart of $\bar{\eta}_m$ evaluated from the additional gradient enhancement equation. Moreover, the equivalent strains of the remaining microplanes are modified with the same ratio of the local to nonlocal largest equivalent strain as follows

$$\bar{\eta}^{mic} = \frac{\bar{\eta}_m}{\eta_m}\eta^{mic}. \tag{54}$$

This means that while the largest equivalent strain is replaced directly by its nonlocal counterpart, the rest of the microplanes are modified with same ratio. Using this method, only one additional degree of freedom is needed, but all the microplanes are

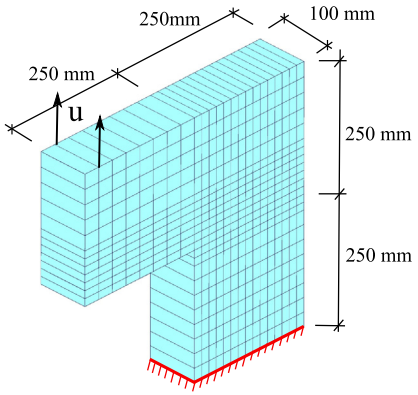

material parameters

Method 1	Method 2
E = 25850 MPa	E = 18000 MPa
$\nu = 0.18$	$\nu = 0.18$
$\alpha = 0.96$	$\alpha = 0.96$
$\beta = 160$	$\beta = 450$
$\gamma_0 = 0.000125$	$\gamma_0 = 0.0002$
$k_r = 10$	$k_r = 10$
c = 1 mm^2	c = 5 mm^2

Fig. 2. Geometry of the L-shaped specimen and material parameters.

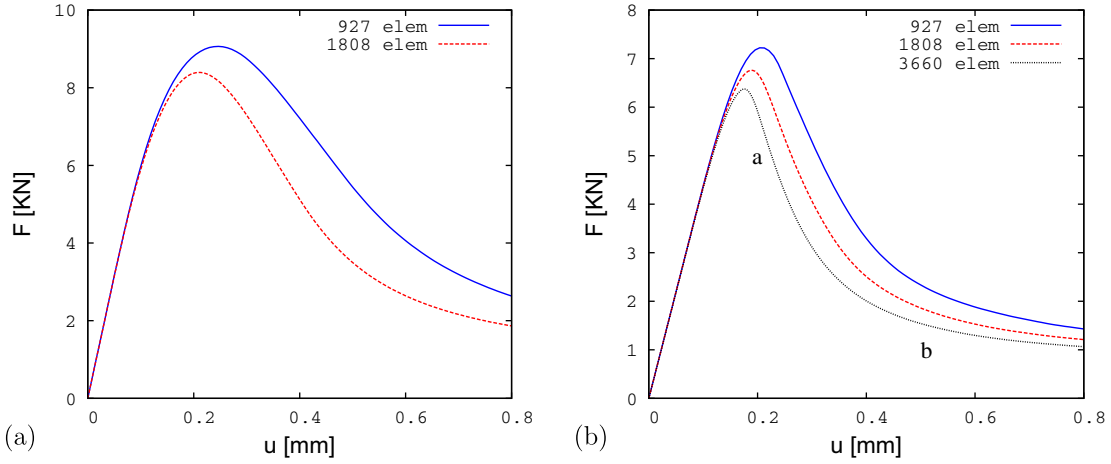

Fig. 3. Comparison of the results for (a) Method 1 and (b) Method 2.

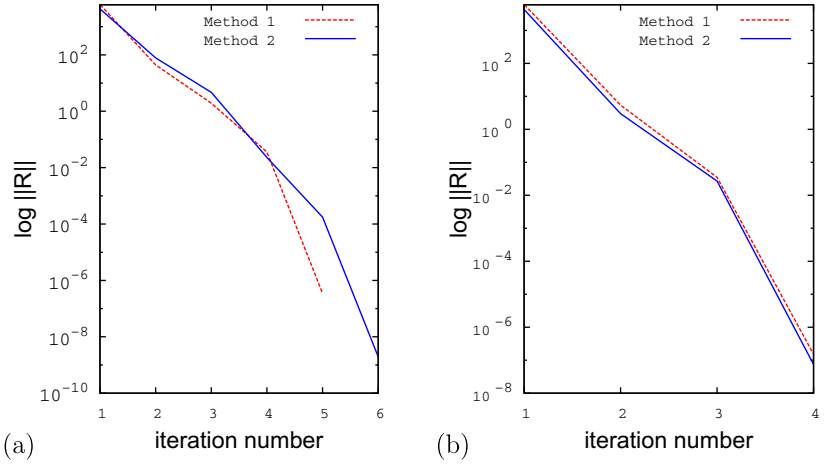

Fig. 4. Convergence rate at different time steps with $\Delta t = 0.1$ s and mesh of 1808 elements mesh, points a and b are shown in Fig. 3(b).

regularized. Moreover, the anisotropic nature of the microplane model is preserved, since the modifying ratio is multiplied by the local equivalent strain of each microplane, i.e. the microplanes are still independent of each other, though the gradient enhancement is driven by one microplane. As can be seen, this method differs from the strain gradient method. First, the equivalent strain now is computed from the local strains,

$$\eta^{mic} = 3k_1\epsilon_V + \sqrt{(3k_1\epsilon_V)^2 + \frac{3}{2}k_2\boldsymbol{\epsilon}_D \cdot \boldsymbol{\epsilon}_D} \tag{55}$$

and then is modified by the ratio $\bar{\eta}_m/\eta_m$ to prevent localization. The history variable driving damage evolution γ^{mic} may now be evaluated as the maximum value of the modified equivalent strain reached in the whole loading history on each microplane

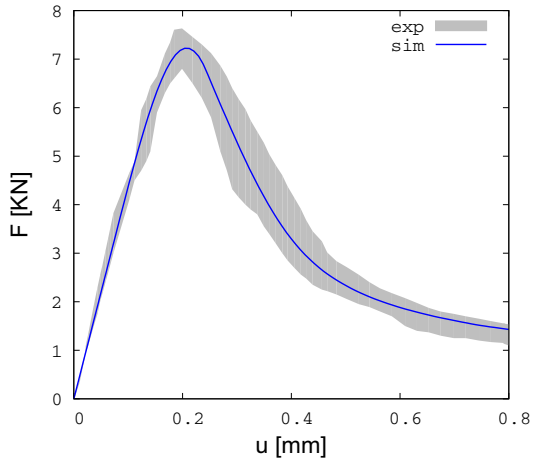

Fig. 5. Comparison of experiments and simulation of the L-shaped specimen test using Method 2.

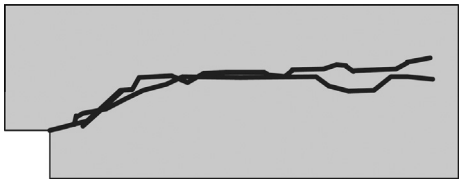

Fig. 6. Experimental crack pattern of the L-shaped specimen test as reported in Winkler (2001).

$$\gamma^{mic}(t) = \max_{\tau \leqslant t}(\gamma_0, \bar{\eta}^{mic}(\tau)) \tag{56}$$

and the damage is evaluated as a function of γ^{mic} with the same exponential function as before, see Eq. (29).

The stress tensor after homogenization takes the same form as in the previous method

$$\boldsymbol{\sigma} = \frac{\partial \Psi^{mac}}{\partial \boldsymbol{\epsilon}} = \frac{3}{4\pi}\int_{\Omega}\left[1 - d^{mic}\right]\left[K^{mic}\boldsymbol{V}\epsilon_V + 2G^{mic}\boldsymbol{Dev}^T \cdot \boldsymbol{\epsilon}_D\right]d\Omega, \tag{57}$$

however, the tangent terms for the new method are different,

$$\mathbb{C} = \frac{\partial \boldsymbol{\sigma}}{\partial \boldsymbol{\epsilon}} = \frac{3}{4\pi}\int_{\Omega}\left[1 - d^{mic}\right]\left[K^{mic}\boldsymbol{V}\otimes\boldsymbol{V} + 2G^{mic}\boldsymbol{Dev}^T \cdot \boldsymbol{Dev}\right]d\Omega - \frac{3}{4\pi}\int_{\Omega}\left[K^{mic}\boldsymbol{V}\epsilon_V + 2G^{mic}\boldsymbol{Dev}^T \cdot \boldsymbol{\epsilon}_D\right]\otimes\frac{\partial d^{mic}}{\partial \boldsymbol{\epsilon}}d\Omega, \tag{58}$$

$$\overline{\mathbb{C}} = \frac{\partial \boldsymbol{\sigma}}{\partial \bar{\eta}_m} = -\frac{3}{4\pi}\int_{\Omega}\frac{\partial d^{mic}}{\partial \bar{\eta}_m}\left[K^{mic}\boldsymbol{V}\epsilon_V + 2G^{mic}\boldsymbol{\epsilon}_D \cdot \boldsymbol{Dev}\right]d\Omega. \tag{59}$$

The required derivatives are

$$\frac{\partial d^{mic}}{\partial \boldsymbol{\epsilon}} = \frac{\partial d^{mic}}{\partial \gamma^{mic}}\frac{\partial \gamma^{mic}}{\partial \eta^{mic}}\left[\frac{\bar{\eta}_m}{\eta_m}\frac{\partial \eta^{mic}}{\partial \boldsymbol{\epsilon}} - \frac{\bar{\eta}_m}{\eta_m^2}\eta^{mic}\frac{\partial \eta_m}{\partial \boldsymbol{\epsilon}}\right], \tag{60}$$

$$\frac{\partial d^{mic}}{\partial \bar{\eta}_m} = \frac{\partial d^{mic}}{\partial \gamma^{mic}}\frac{\partial \gamma^{mic}}{\partial \bar{\eta}^{mic}}\frac{\eta^{mic}}{\eta_m}, \tag{61}$$

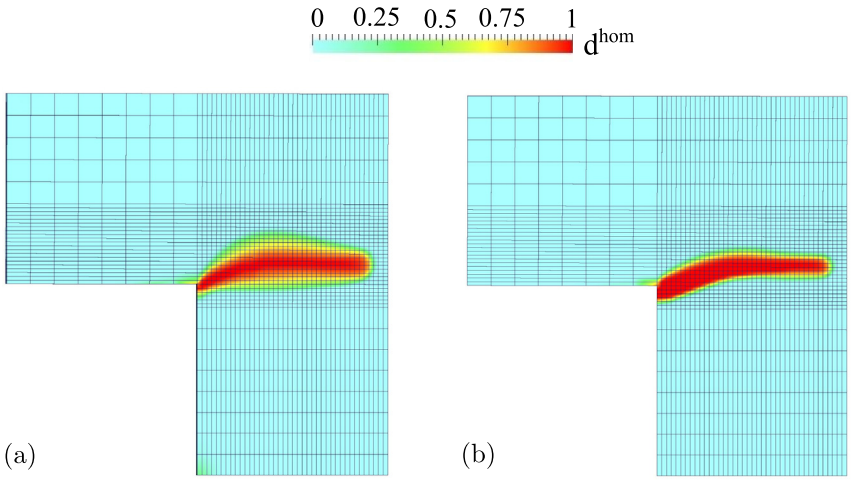

Fig. 7. Damaged zone as predicted by (a) Method 1 and (b) Method 2.

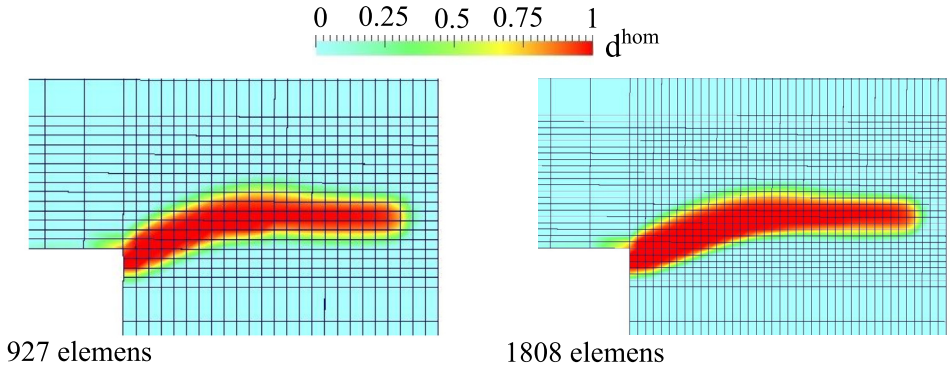

Fig. 8. Mesh objectivity preserved by Method 2.

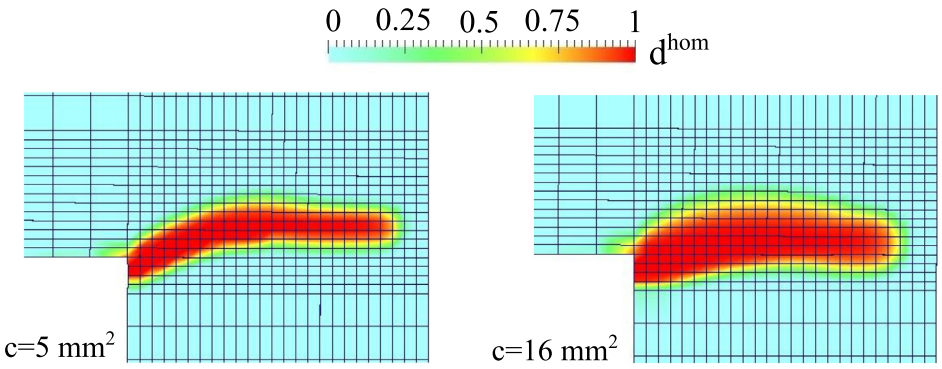

Fig. 9. The effect of gradient parameter c on the size of the damaged zone for Method 2.

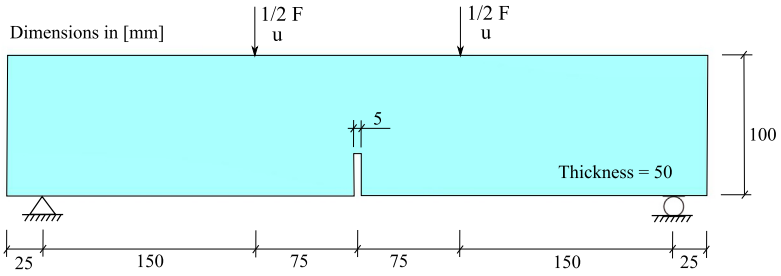

Fig. 10. Geometry and boundary conditions of the four-point bending test.

Table 1
Material parameters used in the four-point bending test.

E	ν	α	β	γ_0	k_r	c
38 [GPa]	0.18	0.94	150	0.00007	10	4 [mm^2]

$$\frac{\partial \eta^{mic}}{\partial \boldsymbol{\epsilon}} = 3k_1\boldsymbol{V} + \frac{1}{2\sqrt{(3k_1\epsilon_V)^2 + \frac{3}{2}k_2\boldsymbol{\epsilon}_D\cdot\boldsymbol{\epsilon}_D}}\left(18k_1^2\epsilon_V\boldsymbol{V} + 3k_2\boldsymbol{Dev}^T\cdot\boldsymbol{\epsilon}_D\right). \tag{62}$$

4. Numerical examples

The two methods explained in the previous sections are implemented within a 3D finite element code with 8-node hexahedral brick element. Next, the simulation results of three commonly used experiments for testing concrete fracture are given.

4.1. L-shaped specimen

The first example deals with testing of an L-shaped concrete specimen, which represents an interesting problem for testing

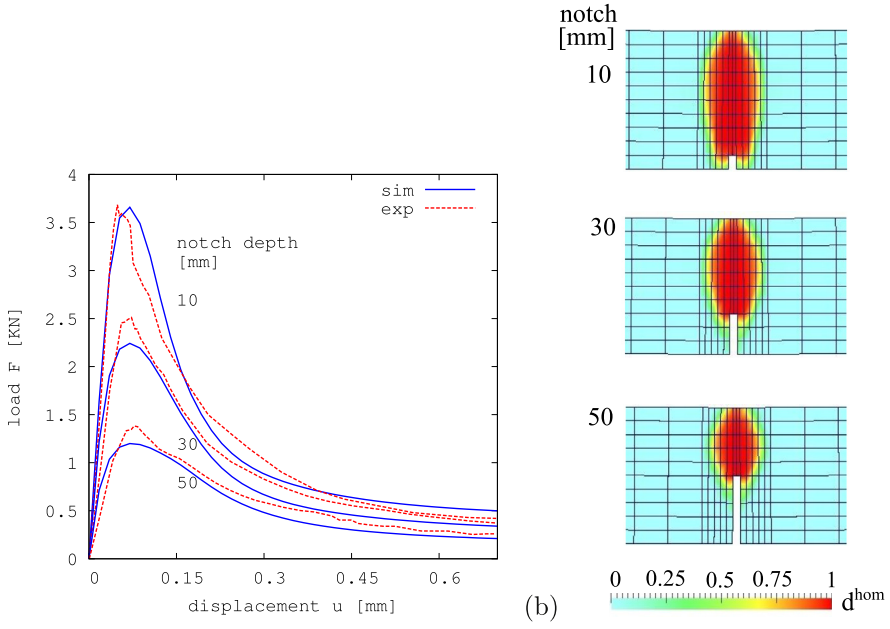

Fig. 11. (a) Experimental and simulated load–displacement curves for the bending test with 3 different notch depths, (b) the corresponding damage distribution (Method 2).

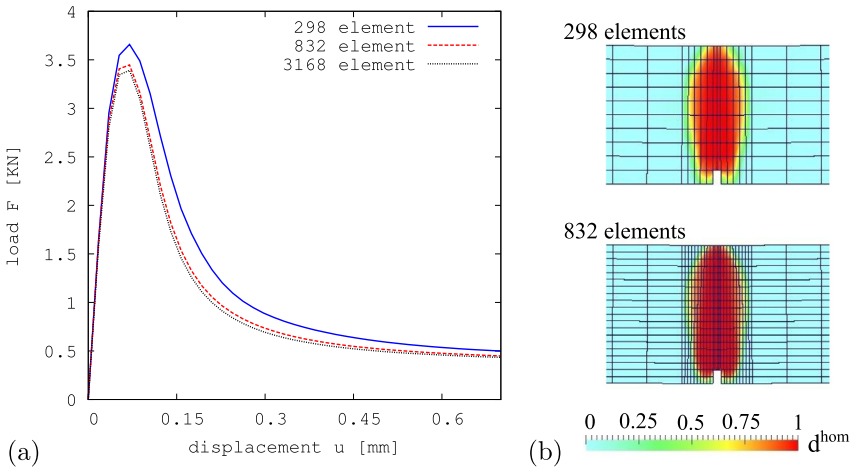

Fig. 12. 4-point bending test with two mesh sizes for notch depth 10 mm (Method 2).

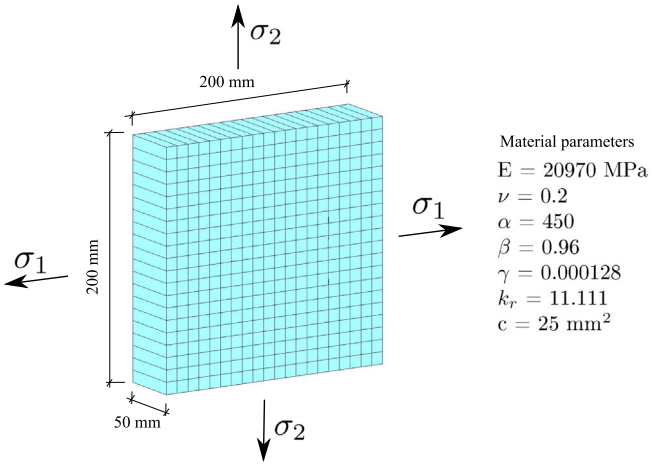

Fig. 13. Geometry and material parameters for the biaxial test.

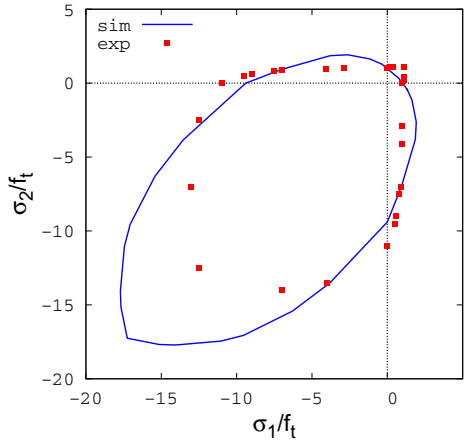

Fig. 14. Biaxial strength envelope and experimental data.

crack propagation and fracture of concrete and which is particularly suitable for the verification of numerical models, since it involves mixed-mode fracture (Ožbolt and Sharma, 2012). The experimental data which is simulated is taken from Winkler et al. (2001). Fig. 2 shows the geometry of the test specimen. It is fixed at the bottom, and the load is applied at the shown position using displacement control at a rate of 0.04 mm/s. In the following, the strain gradient method will be referred as *Method 1*, while the new method is referred as *Method 2*. The test is performed using two different meshes to check for localization and mesh dependency. The material parameters for Method 1 are taken from Leukart (2005), while the parameters for Method 2 are identified to fit the experiments. The parameters for both methods are shown in Fig. 2.

The comparison of the behavior of the regularized models with two different meshes is shown in Fig. 3 for the two methods. As can be observed, both methods are capable of limiting localization and restoring mesh objectivity. Moreover, quadratic convergence is achieved in both cases as shown in Fig. 4. The capability of the new method to fit the experimental data is demonstrated in Fig. 5. The experimental crack pattern is shown in Fig. 6. Fig. 7 shows and compares the crack pattern as observed for the two methods. While both methods reproduce to a good extent the general crack path, a difference is observed between them. Due to the fact that there are 21 independent damage variables d^{mic}, a scalar damage measure d^{hom} is calculated to have a representation of the total damage at each material point. The homogenized damage d^{hom} is given as

$$d^{hom} = \frac{\frac{3}{4\pi}\int_\Omega d^{mic} d\Omega}{\frac{3}{4\pi}\int_\Omega d\Omega}. \tag{63}$$

The mesh objectivity achieved by Method 2 is demonstrated in Fig. 8. Different mesh sizes result in similar size and shape of the damaged zone. The effect of the gradient parameter c is shown in Fig. 9. A larger value of c produces a larger inelastic zone, however, the values of the gradient parameter of the two methods are totally different. Method 2 requires larger c to produce a damaged zone with equal size as Method 1. It is clear that the decisive parameter in this method is the characteristic length $\sqrt{c}$. However, there is no explicit relation between it and the macroscopic material properties, i.e. changing it will lead to a change in macroscopic material parameters, and it has been observed that the same experiments may be fitted with different length scales. These facts indicate that this length is not a material parameter that can be correlated to the material properties only. It is now clear that, this length is influenced by other factors, such as the type of problem. It changes from tensile fracture to shear failure. It is also confirmed that it is not constant but a function depending on stress and strain fields (Ožbolt and Bažant, 1996), and decreases at larger strains. However, this does not hinder the practical application of the this type of models, since a good calibration of the length scale may be obtained

by conducting a notched fracture test of specimens with different sizes (Caner and Bažant, 2013b).

4.2. Four-point bending test

A notched beam of plain concrete is tested at four-point bending conditions. The experimental data are taken from Hordijk (1991). The specimen's geometry and boundary conditions are shown in Fig. 10. The specimen was tested with different notch depths 10, 30 and 50 mm. The finite element model is discretized with 298 brick elements, with a finer mesh near the notch. The material parameters are shown in Table 1. The elastic properties of the material are taken from the same source as the experiments (Hordijk, 1991), while the rest of the parameters are identified to fit the curves. The same set of parameters is used to fit the results of the three notch depths and very good agreement is observed between simulation and experiments, see Fig. 11. Furthermore, mesh objectivity is checked and confirmed by two finer meshes with 832 and 3168 elements, see Fig. 12. It should be noted that gradient models require the use of relatively fine meshes, in order to have a correct nonlocal interaction, since the localized zone cannot be smaller than the size of one element.

4.3. Biaxial strength envelope

In order to test the model further in the case of different directions of damage, a biaxial failure envelope of concrete is simulated. Kupfer et al. (1969) tested a set of concrete panels of 200 mm × 200 mm and 50 mm thickness, subjected to various biaxial load conditions, as shown on Fig. 13. The tested concrete has the following properties: Young's modulus 20.970 MPa, Poisson's ratio 0.2 and tensile strength $f_t = 2.608$ MPa. The material parameters used are listed in Fig. 13. The test is modeled with the boundary conditions, such that to produce a homogeneous distribution of the stress field in the panel. The test is driven by displacements with different magnitudes in two directions and the ultimate stress reached and its corresponding lateral stress is obtained. The strength envelop obtained is shown in Fig. 14, and the experimental data is plotted in the same figure. The results show an overestimation of the concrete strength under biaxial compression and shear, this is related to the used modified von Mises equivalent strain law. However, the gradient formulation is still working correctly also under different directions of damage.

5. Conclusions

The present work demonstrates numerically that implicit gradient enhancement is a powerful tool of regularization for microplane damage models, and introduces a new efficient method of enhancement. A microplane damage model based on a thermodynamically consistent approach and a volumetric–deviatoric split is implemented and enhanced with two different implicit gradient enhancement methods. The damage law used is mainly suitable for concrete-like materials, where distinction between compression and tension is incorporated and the exponential damage law can simulate the long tail in the load displacement curve. The version of the implicit gradient enhancement found in literature, which is based on enhancing the strain tensor is explained, and then, a new method which enhances the equivalent strain is derived for the case of the microplane model. Both methods are implemented within an implicit finite element code, and their behavior is tested against experiments, as well as against each other. Both methods show the ability to regularize the solution and eliminate the pathological mesh dependency of the local model. Moreover, both methods can simulate the crack pattern of mixed mode fracture, though there is a difference between the size and shape of the damaged zone. The new method shows a very good capability in fitting experimental data as observed in the L-shaped specimen test as well as in the 4-point bending test. Furthermore, an important advantage of the new method is the substantial reduction of computational time by reducing the extra degrees of freedom.

Future work may be dedicated to identifying the gradient parameter with more experiments as well as the possibility of using a transient evolving gradient parameter to have a more accurate crack patterns. Moreover, regularizing microplane plasticity models with an implicit gradient enhancement is also an important topic to consider.

Acknowledgments

The authors gratefully acknowledge the financial support of ANSYS Inc., Canonsburg, USA.

Appendix A

See Table 2.

Table 2
Integration over a sphere surface with 21 integration points – coordinates and weight coefficients.

Mic	*x*-Coordinate	*y*-Coordinate	*z*-Coordinate	Weight w^{mic}
1	0.187592474085	0.000000000000	0.982246946377	0.1190476190478
2	0.794654472292	−0.525731112119	0.303530999103	0.1190476190478
3	0.794654472292	0.525731112119	0.303530999103	0.1190476190478
4	0.187592474085	−0.850650808352	−0.491123473188	0.1190476190478
5	0.794654472292	0.000000000000	−0.607061998207	0.1190476190478
6	0.187592474085	0.850650808352	−0.491123473188	0.1190476190478
7	0.577350269190	−0.309016994375	0.755761314076	0.1523809523808
8	0.577350269190	0.309016994375	0.755761314076	0.1523809523808
9	0.934172358963	0.000000000000	0.356822089773	0.1523809523808
10	0.577350269190	−0.809016994375	−0.110264089708	0.1523809523808
11	0.934172358963	−0.309016994375	−0.178411044887	0.1523809523808
12	0.934172358963	0.309016994375	−0.178411044887	0.1523809523808
13	0.577350269190	0.809016994375	−0.110264089708	0.1523809523808
14	0.577350269190	−0.500000000000	−0.645497224368	0.1523809523808
15	0.577350269190	0.500000000000	−0.645497224368	0.1523809523808
16	0.356822089773	−0.809016994375	0.467086179481	0.1523809523808
17	0.356822089773	0.000000000000	−0.934172358963	0.1523809523808
18	0.356822089773	0.809016994375	0.467086179481	0.1523809523808
19	0.000000000000	−0.500000000000	0.866025403784	0.1523809523808
20	0.000000000000	−0.500000000000	−0.866025403784	0.1523809523808
21	0.000000000000	−1.000000000000	0.000000000000	0.1523809523808

References

Bažant, Z., 1991. Why continuum damage is nonlocal: micromechanics arguments. J. Eng. Mech. 117, 1070–1087.

Bažant, Z., Caner, F., Carol, I., Adley, M., Akers, S., 2000. Microplane model m4 for concrete. I: Formulation with work-conjugate deviatoric stress. J. Eng. Mech. 126, 944–953.

Bažant, Z., Di Luzio, G., 2004. Nonlocal microplane model with strain-softening yield limits. Int. J. Solids Struct. 41, 7209–7240.

Bažant, Z., Oh, B.H., 1986. Efficient numerical integration on the surface of a sphere. ZAMM – J. Appl. Math. Mech./Zeit. Angew. Math. Mech. 66, 37–49.

Bažant, Z., Ozbolt, J., 1990. Nonlocal microplane model for fracture, damage, and size effect in structures. J. Eng. Mech. 116, 2485–2505.

Bažant, Z., Prat, P.C., 1988. Microplane model for brittle-plastic material: I. Theory. J. Eng. Mech. 114, 1672–1688.

Caner, F., Bažant, Z., 2013a. Microplane model m7 for plain concrete. I: Formulation. J. Eng. Mech. 139, 1714–1723.

Caner, F., Bažant, Z., 2013b. Microplane model m7 for plain concrete. II: Calibration and verification. J. Eng. Mech. 139, 1724–1735.

Geers, M.G.D., de Borst, R., Brekelmans, W.A.M., Peerlings, R.H.J., 1998. Strain-based transient-gradient damage model for failure analyses. Comput. Methods Appl. Mech. Eng. 160, 133–153.

Geers, M.G.D., Peerlings, R.H.J., Brekelmans, W.a.M., Borst, R.d., 2000. Phenomenological nonlocal approaches based on implicit gradient-enhanced damage. Acta Mech. 144, 1–15.

Hordijk, D., 1991. Local Approach to Fatigue of Concrete (Ph.D. thesis). Delft University of Technology.

Jirásek, M., Patzák, B., 2002. Consistent tangent stiffness for nonlocal damage models. Comput. Struct. 80, 1279–1293.

Kuhl, E., Ramm, E., de Borst, R., 2000. Anisotropic gradient damage with the microplane model. Comput. Methods Appl. Mech. Eng. 183, 87–103.

Kupfer, H., Hilsdorf, H., Rusch, H., 1969. Behavior of concrete under biaxial stresses. ACI J. Proc. 66, 656–666.

Leukart, M., 2005. Kombinierte Anisotrope Schädigung und Plastizität bei Kohäsiven Reibungsmaterialien (Ph.D. thesis). Institut für Baustatik der Universität Stuttgart.

Luzio, G.D., 2007. A symmetric over-nonlocal microplane model m4 for fracture in concrete. Int. J. Solids Struct. 44, 4418–4441.

Ožbolt, J., Bažant, Z., 1996. Numerical smeared fracture analysis: nonlocal microcrack interaction approach. Int. J. Numer. Methods Eng. 39, 635–661.

Ožbolt, J., Sharma, A., 2012. Numerical simulation of dynamic fracture of concrete through uniaxial tension and l-specimen. Eng. Fract. Mech. 85, 88–102.

Peerlings, R.H.J., Geers, M.G.D., de Borst, R., Brekelmans, W.A.M., 2001. A critical comparison of nonlocal and gradient-enhanced softening continua. Int. J. Solids Struct. 38, 7723–7746.

Saroukhani, S., Vafadari, R., Simone, A., 2013. A simplified implementation of a gradient-enhanced damage model with transient length scale effects. Comput. Mech. 51, 899–909.

de Vree, J., Brekelmans, W., 1995. Comparison of nonlocal approaches in continuum damage mechanics. Comput. Struct. 55, 581–588.

Winkler, B., Hofstetter, G., Niederwanger, G., 2001. Experimental verification of a constitutive model for concrete cracking. Proc. Inst. Mech. Eng., Part L: J. Mater. Des. Appl. 215, 75–86.

Winkler, B.J., 2001. Traglastuntersuchungen von Unbewehrten und Bewehrten Betonstrukturen auf der Grundlage eines Objektiven Werkstoffgesetzes für Beton (Ph.D. thesis). University of Innsbruck.